# Dependence of LBNE long-baseline neutrino oscillation sensitivities on knowledge of neutrino oscillation parameters

April 17, 2014

**Abstract**

The sensitivity of long-baseline neutrino oscillation experiments depends significantly on the true values of neutrino oscillation parameters. The purpose of this paper is to document the dependence of LBNE's sensitivity to determination of the neutrino mass hierarchy, discovery of CP violation, and determination of the $\theta_{23}$ octant on the central values of neutrino oscillation parameters and on how well these parameters are determined by external constraints. This information will be useful for adjusting expectations for LBNE sensitivity as new measurements of oscillation parameters become available and for understanding the value of additional pre-LBNE measurements of oscillation parameters. We find that xxx.

## 1 Introduction

It is well-established experimentally that the flavor composition of neutrinos change as they propagate[1]. In the three-neutrino framework, the three flavor states $(\nu_e, \nu_\mu, \nu_\tau)$ are superpositions of the three mass states $(\nu_1, \nu_2, \nu_3)$. The PMNS[2, 3, 4] matrix describes this mixing with three mixing angles $(\theta_{12}, \theta_{23}, \theta_{13})$, which have all been measured experimentally, and a CP-violating phase, $\delta_{CP}$, which is unknown. Measurement of a value of $\delta_{CP}$ not equal to zero or pi would be the first observation of CP violation in the neutrino sector. The differences between the mass states, $\Delta m^2_{21}$ and $|\Delta m^2_{31}|$, have also been measured. The case in which $\Delta m^2_{31}$ is greater than zero is referred to as "normal hierarchy" (NH) and the opposite case is called "inverted hierarchy" (IH); the true neutrino mass hierarchy has not yet been determined. The measured value of $\theta_{23}$ is near to 45°; if it is exactly 45°, which would indicate that $\nu_\mu$ and $\nu_\tau$ have equal contributions from $\nu_3$, that could be evidence for a previously unknown symmetry. The $\theta_{23}$ octant, i.e., whether $\theta_{23}$ is less than, greater than, or equal to 45°, is unknown.

These three measurements – determination of the neutrino mass hierarchy (MH), discovery of CP violation (CPV), and determination of the $\theta_{23}$ octant – are among the primary physics goals of LBNE, the Long Baseline Neutrino Experiment [5]. LBNE will use a combined analysis of $\nu_e$ appearance and $\nu_\mu$ disappearance in a muon-neutrino beam to study neutrino oscillation. The experiment will consist of a muon-neutrino beam from Fermilab to Sanford Underground Research Facility (SURF), a baseline of 1300 km, and a massive underground far detector. The experiment will make use of protons from Fermilab's Main Injector and a new muon-neutrino beam line will be constructed. The far detector will be a liquid argon time projection chamber (LAr TPC) with an integrated photon detection system. For the sensitivities presented in this paper, we study both a 10-kt and a 35-kt fiducial-volume far detector. We assume a 1.2-MW, 80-GeV beam with six years of exposure, divided equally between neutrino and antineutrino running. We also present sensitivities as a function of exposure in kt.MW.years.

## 2 Neutrino Oscillation in the Three-flavor Paradigm

The oscillation probability of $\nu_{\mu,e} \to \nu_{e,\mu}$ through matter, in a constant density approximation, keeping terms up to second order in $\alpha \equiv |\Delta m^2_{21}|/|\Delta m^2_{31}|$ and $\sin^2\theta_{13}$, is [6, 1]:

$$P(\nu_\mu \to \nu_e) \cong P(\nu_e \to \nu_\mu) \cong P_0 + \underbrace{P_{\sin\delta}}_{\text{CP violating}} + P_{\cos\delta} + P_3 \tag{1}$$

where

$$P_0 = \sin^2\theta_{23}\frac{\sin^2 2\theta_{13}}{(A-1)^2}\sin^2[(A-1)\Delta], \tag{2}$$

$$P_{\sin\delta} = -\alpha\frac{8J_{cp}}{A(1-A)}\sin\Delta\sin(A\Delta)\sin[(1-A)\Delta], \tag{3}$$

$$P_{\cos\delta} = \alpha\frac{8J_{cp}\cot\delta_{CP}}{A(1-A)}\cos\Delta\sin(A\Delta)\sin[(1-A)\Delta], \tag{4}$$

$$P_3 = \alpha^2\cos^2\theta_{23}\frac{\sin^2 2\theta_{12}}{A^2}\sin^2(A\Delta), \tag{5}$$

$$\tag{6}$$

and where

$$\Delta = \Delta m^2_{31}L/4E, \tag{7}$$

$$A = \sqrt{3}G_F N_e 2E/\Delta m^2_{31}, \text{ and} \tag{8}$$

$$J_{CP}^{\text{PMNS}} \equiv \frac{1}{8}\sin 2\theta_{12}\sin 2\theta_{13}\sin 2\theta_{23}\cos\theta_{13}\sin\delta_{CP}. \tag{9}$$

In the above, the CP phase $\delta_{CP}$ appears (via $J_{cp}$) in the expressions for $P_{\sin\delta}$ (the CP-odd term) which switches sign in going from $\nu_\mu \to \nu_e$ to the $\overline{\nu}_\mu \to \overline{\nu}_e$ channel, and $P_{\cos\delta}$ (the CP-conserving term) which does not. The matter effect also introduces a neutrino-antineutrino asymmetry, the origin of which is simply the presence of electrons and absence of positrons in the Earth.

A global fit to all available experimental data is described in [7]; the central values, $1\sigma$ and $3\sigma$ ranges of the fit, and $1\sigma$ precision are shown in Table 1. The best-fit values are somewhat different for normal and inverted hierarchy. The fit results for each parameter in the global fit are shown graphically as N$\sigma$ contours in Fig. 1.

## 3 Calculation of Experimental Sensitivities using GLoBES

The sensitivity of LBNE to the mass hierarchy, CP violation, and the octant of $\theta_{23}$ are calculated using the GLoBES [8, 9] package to simulate the detector response using "true" values of the oscillation parameters based on the global fit, smearing based on a simple resolution or on a GENIE[10] simulation, and detector efficiency values based on results from ICARUS[11] and earlier simulation efforts. The oscillation parameters used in GLoBES are shown in Table 2. The detector efficiencies and the energy resolution for $\nu_e$ charged current (CC) and $\nu_\mu$ CC interactions used in GLoBES are shown in Table 3. The smearing matrices for $\nu_\mu$ neutral current (NC) and $\nu_\tau$ interactions are shown in Fig. 2.

Estimates of experimental sensitivity are obtained in GLoBES by simultaneously fitting the $\nu_\mu \to \nu_\mu$, $\overline{\nu}_\mu \to \overline{\nu}_\mu$, $\nu_\mu \to \nu_e$, and $\overline{\nu}_\mu \to \overline{\nu}_e$ oscillated spectra, examples of which are shown in Figure 3. In these calculations, experimental sensitivity is quantified using $\Delta\chi^2$ parameters, which are determined

Table 1: Blah

| Parameter | Hierarchy | Best Fit | $1\sigma$ Range | $3\sigma$ Range | $1\sigma$ Precision |
|---|---|---|---|---|---|
| $\delta m^2/10^{-5}$ eV$^2$ | NH/IH | 7.54 | 7.32-7.80 | 6.99-8.18 | 2.6% |
| $\sin^2\theta_{12}/10^{-1}$ | NH/IH | 3.08 | 2.91-3.25 | 2.59-3.59 | 5.4% |
| $\Delta m^2/10^{-3}$ eV$^2$ | NH | 2.44 | 2.38-2.52 | 2.22-2.66 | 3.0% |
| | IH | 2.40 | 2.33-2.47 | 2.17-2.61 | 3.1% |
| $\sin^2\theta_{13}/10^{-2}$ | NH | 2.34 | 2.16-2.56 | 1.77-2.97 | 8.5% |
| | IH | 2.39 | 2.18-2.60 | 1.78-3.00 | 8.5% |
| $\sin^2\theta_{23}/10^{-1}$ | NH | 4.25 | 3.98-4.54 | 3.57-6.41 | 11.1% |
| | IH | 4.37 | 4.08-4.96 $\oplus$ 5.31-6.10 | 3.63-6.59 | 12.3% |
| $\delta/\pi$ | NH | 1.39 | 1.12-1.72 | — | — |
| | IH | 1.35 | 0.96-1.59 | — | — |

Table 2: Oscillation parameter inputs used in GLoBES sensitivity calculations. Central values are taken from the global fit in [7]. Angles are in radians. Relative uncertainty is defined using 1/6 of the full $3\sigma$ range from [7]. In the case of $\theta_{13}$, the relative uncertainty is based on the current systematic uncertainty in $\sin^2 2\theta_{13}$ from Daya Bay [12] as an approximation of the ultimate precision of the current generation of reactor experiments.

| Parameter | Hierarchy | Central Value | Relative Uncertainty |
|---|---|---|---|
| $\Delta m^2_{21}/10^{-5}$ eV$^2$ | NH/IH | 7.54 | 3% |
| $\theta_{12}$ | NH/IH | 0.588 | 3% |
| $\Delta m^2_{31}/10^{-3}$ eV$^2$ | NH | 2.48 | 3% |
| | IH | -2.36 | 3% |
| $\theta_{13}$ | NH | 0.154 | 3% |
| | IH | 0.155 | 3% |
| $\theta_{23}$ | NH | 0.710 | 7% |
| | IH | 0.722 | 7% |
| $\delta_{CP}$ | NH/IH | scan | no constraint |

by comparing the predicted spectra for various scenarios. These quantities are defined, differently for neutrino MH, CP-violation, and octant sensitivity, to be:

$$\Delta\chi^2_{MH} = |\chi^2_{MH^{test}=IH} - \chi^2_{MH^{test}=NH}|, \quad (10)$$

$$\Delta\chi^2_{CPV} = \min\left(\Delta\chi^2_{CP}(\delta^{test}_{CP}=0), \Delta\chi^2_{CP}(\delta^{test}_{CP}=\pi)\right), \text{ where} \quad (11)$$

$$\Delta\chi^2_{CP} = \chi^2_{\delta^{test}_{cp}} - \chi^2_{\delta^{true}_{CP}}, \text{ and} \quad (12)$$

$$\Delta\chi^2_{octant} = |\chi^2_{\theta^{test}_{23}>45^\circ} - \chi^2_{\theta^{test}_{23}<45^\circ}|. \quad (13)$$

These sensitivities are evaluated separately for true NH and IH. Since the true value of $\delta_{CP}$ is unknown, a scan is performed over all possible values of $\delta^{true}_{CP}$. For the case of the octant sensitivity, the value of $\theta_{23}$ in the "wrong" octant is constrained only to have a value within the "wrong" octant, i.e., it is not required to have the same value of $\sin^2 2\theta_{23}$ as the true value. The individual $\chi^2$ values are calculated

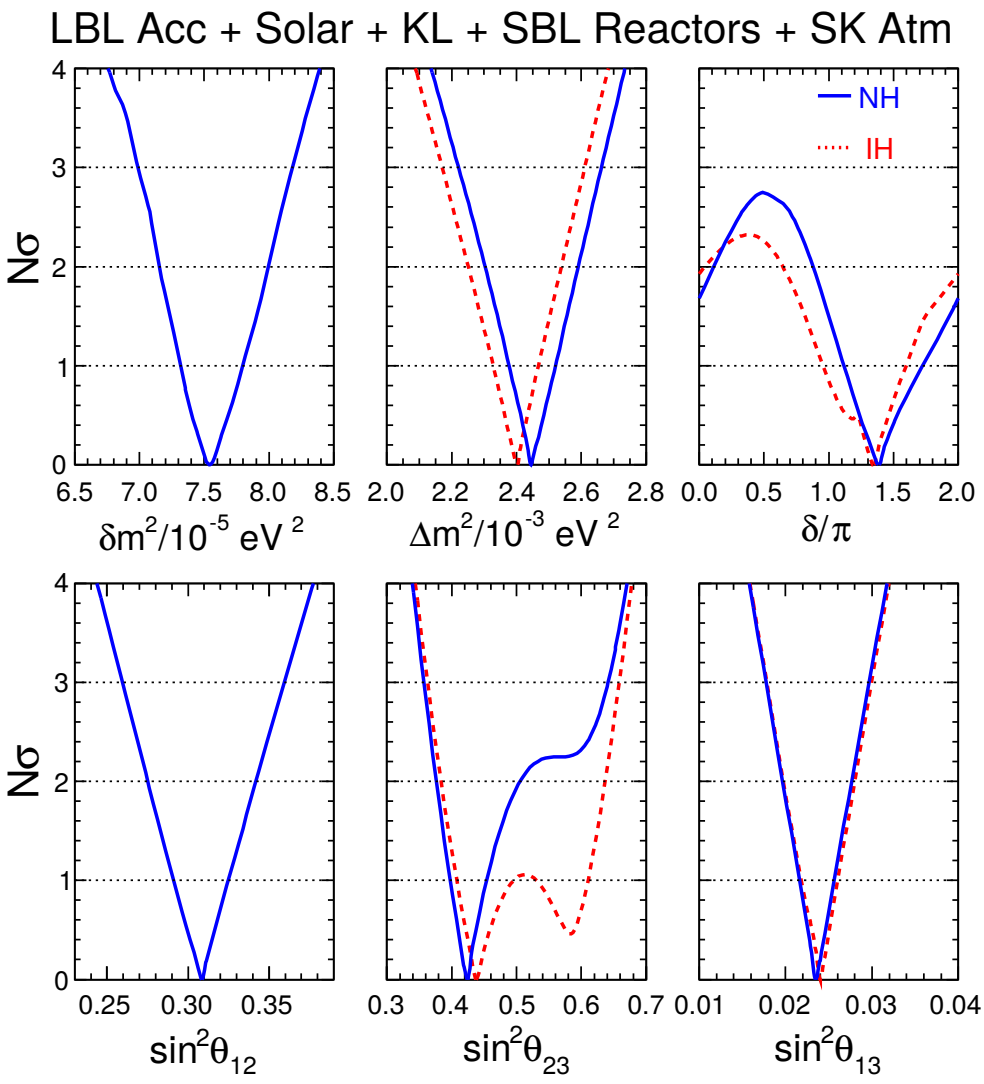


Figure 1: Results of the 2013 global analysis from Capozzi *et al.* shown as N$\sigma$ bounds on the six parameters governing three $\nu$ flavor oscillations. Blue (solid) and red (dashed) curves refer to NH and IH, respectively. Figure is from [7].

using

$$\chi^2(\mathbf{n}^{true}, \mathbf{n}^{test}, f) = 2 \sum_i^{N_{reco}} (n_i^{true} ln \frac{n_i^{true}}{n_i^{test}(f)} + n_i^{test}(f) - n_i^{true}) + f^2, \tag{14}$$

where $\mathbf{n}$ are event rate vectors in $N_{reco}$ bins of reconstructed energy and $f$ represents a nuisance parameter to be profiled. Nuisance parameters include the values of mixing angles, mass splittings, and signal and background normalization. The nuisance parameters are constrained by Gaussian priors; in the case of the oscillation parameters, the Gaussian prior has standard deviation determined by taking 1/6 of the $3\sigma$ range allowed by the global fit [13].

LBNE's sensitivity to MH and CPV is based on observation of the neutrino-antineutrino asymmetry,

$$A_{CP} = \frac{P(\nu_\mu \to \nu_e) - P(\overline{\nu}_\mu \to \overline{\nu}_e)}{P(\nu_\mu \to \nu_e) + P(\overline{\nu}_\mu \to \overline{\nu}_e)}. \tag{15}$$

Table 3: Signal and background effienciencies, normalization uncertainties, and energy resolutions, which are obtained from ICARUS and earlier simulation efforts, used in the GLoBES sensitivity calculations.

| Parameter | Value Used for LBNE Sensitivities |
|---|---|
| | For $\nu_e$-CC appearance |
| $\nu_e$-CC efficiency | 80% |
| $\nu_\mu$-NC mis-identification rate | 1% |
| $\nu_\mu$-CC mis-identification rate | 1% |
| Other background | 0% |
| Signal normalization error | 1% |
| Background normalization error | 5% |
| | For $\nu_\mu$-CC disappearance |
| $\nu_\mu$-CC efficiency | 85% |
| $\nu_\mu$-NC mis-identification rate | 1% |
| Other background | 0% |
| Signal normalization error | 5% |
| Background normalization error | 10% |
| | Neutrino Energy Resolutions |
| $\nu_e$ CC energy resolution | $15\%/\sqrt{E(GeV)}$ |
| $\nu_\mu$ CC energy resolution | $15\%/\sqrt{E(GeV)}$ |

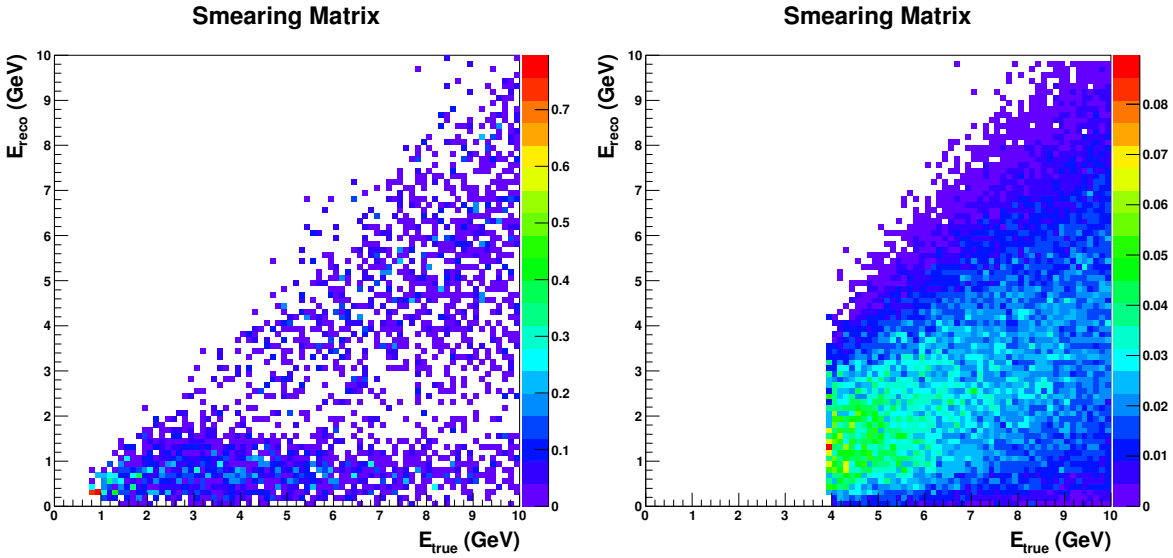


Figure 2: $\nu_\mu$ NC (left) and $\nu_\tau$ energy smearing matrices, produced using a GENIE simulation, used in the GLoBES senstivitiy calculations.

This asymmetry contains contributions both from the different effective masses of neutrinos and antineutrinos as they propagate in matter and from CP violation related to $\delta_{CP}$. Figure 4 shows the total asymmetry at 1300 km for the first and second oscillation nodes, for both NH and IH. There is a nearly degenerate value for the asymmetries at $\delta_{CP} \sim \pi/2$, true NH and at $\delta_{CP} \sim -\pi/2$, true IH in the first oscillation node. This is the reason for the decrease in MH sensitivity for long-baseline

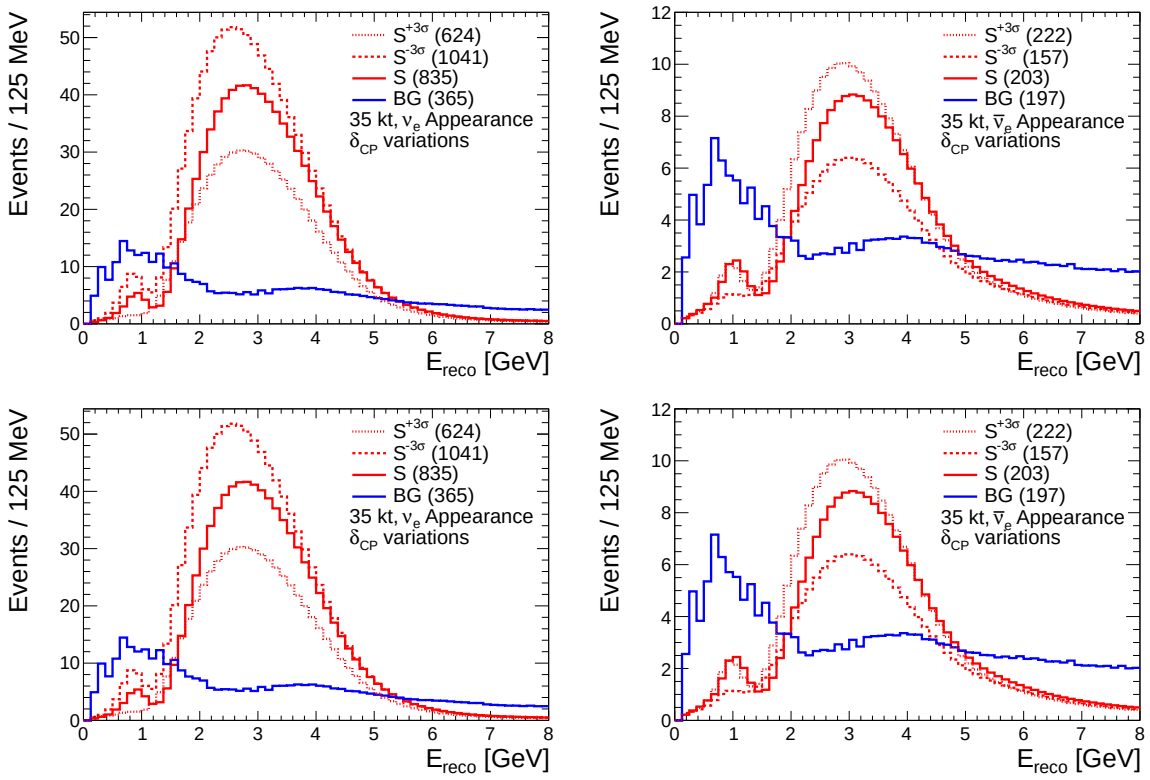


Figure 3: FIXME: Get real disappearance plots. Examples of spectra produced by GLoBES for a 35-kt LArTPC with 3 years of exposure in an 80-GeV, 1.2-MW beam, for the case of true NH. $\nu_\mu$ disappearance (top left), $\overline{\nu}_\mu$ disappearance (top right), $\nu_e$ appearance (bottom left), and $\overline{\nu}_e$ appearance (bottom right). The effect of varying the true value of $\delta_{CP}$ from -$\pi/2$ to zero to $\pi/2$ is shown. The total background, which does not depend on $\delta_{CP}$, is overlaid on the signal. The total number of signal and background events are indicated in parenthesis.

experiments in the region near $\delta_{CP} \sim \pi/2$. Shorter baseline experiments also see degradation of CPV sensitivity in this region [**?**], but in LBNE, the MH will be resolved with sufficient precision that the CPV sensitivity is not strongly affected by degeneracies. Fig. 4 also highlights the critical importance of experimental access to the second oscillation node, where the CP asymmetry is larger, so no such degeneracy with the matter effect is present.

## 4 Sensitivity Dependence on $\theta_{13}$

Figure 5 shows the variation in $\nu_e$ and $\overline{\nu}_e$ appearance signal when the true value of $\theta_{13}$ is varied within its $3\sigma$ allowed range. The effect of increasing $\theta_{13}$ is an increase in event rate with no change to the spectral shape. This can be understood by inspection of Equation 1, in which $P_0$ includes a factor of $\sin^2 2\theta_{13}$. Figure 6 shows the variation in MH and CPV sensitivity when $\theta_{13}$ is varied within its $1\sigma$ and $3\sigma$ allowed range. In each case, the nominal relative constraints on all oscillation parameters, including $\theta_{13}$, are applied and the normalization constraints are the nominal 1% for signal and 5% for background. The increased statistics from increasing $\theta_{13}$ provides a modest increase in MH sensitivity for both true NH and IH. The CPV sensitivity does not improve significantly. The slightly larger increase in sensitivity in IH compared to NH can be understood because the statistics in true IH are signficantly lower than in true IH, so increasing the sample size has a larger effect. FIXME: Seems

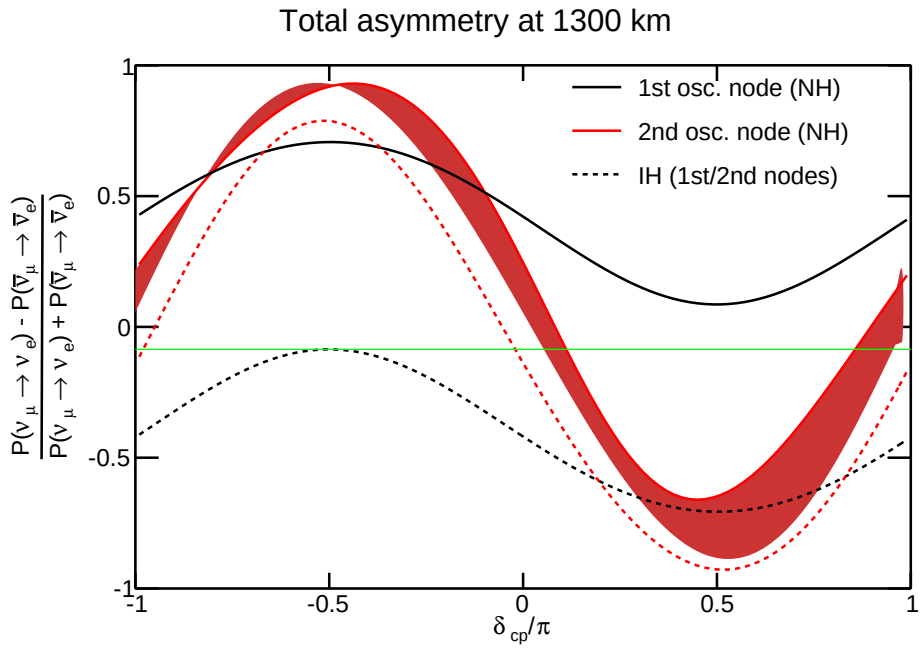


Figure 4: Neutrino-antineutrino asymmetry as a function of $\delta_{CP}$ for the first (black) and second (red) oscillation nodes, for NH (solid) and IH (dashed), at the LBNE baseline of 1300 km.

believeable but is this true?

## 5 Sensitivity Dependence on $\theta_{23}$

Figure 7 shows the variation in $\nu_e$ and $\overline{\nu}_e$ appearance signal when the true value of $\theta_{23}$ is varied within its $3\sigma$ allowed range. Increasing the true value of $\theta_{23}$ results in an increase in $\nu_e$ appearance signal; this can be understood by inspection of Equation 1, where $P_0$ includes a factor of $\sin^2\theta_{23}$. Figure 8 shows the variation in MH and CPV sensitivity when $\theta_{23}$ is varied within its $1\sigma$ and $3\sigma$ allowed range. In each case, the nominal relative constraints on all oscillation parameters, including $\theta_{23}$, are applied and the normalization constraints are the nominal 1% for signal and 5% for background. It is clear from these figures that LBNE sensitivity to MH and CPV depends rather strongly on the true value of $\theta_{23}$. As $\theta_{23}$ increases, sensitivity to CPV decreases while sensitivity to MH increases. Starting from Equation 1, one can show that the CP asymmetry measured by LBNE depends directly on $\theta_{23}$:

$$\mathcal{A}_{CP} \sim \frac{\cos\theta_{23}\sin 2\theta_{12}\sin\delta_{CP}}{\sin\theta_{23}\sin\theta_{13}}\left(\frac{\Delta m^2_{21}L}{4E_\nu}\right) + \text{matter effects.} \tag{16}$$

This asymmetry decreases with increasing $\theta_{23}$; sensitivity decreases because the quantity being measured is smaller. The decrease in CP asymmetry also explains the increase in MH sensitivity. The limiting factor to MH sensitivity in the region where $\delta_{CP} > 0$ is the degeneracy between CP and matter asymmetries, described in Section 2. The decrease in CP asymmetry with increasing $\theta_{23}$ partially breaks this degeneracy, increasing MH sensitivity. This effect is illustrated by the spectra in Fig. 9. The explicit dependence of the MH sensitivity on $\theta_{23}$ is shown in Fig. **??**.

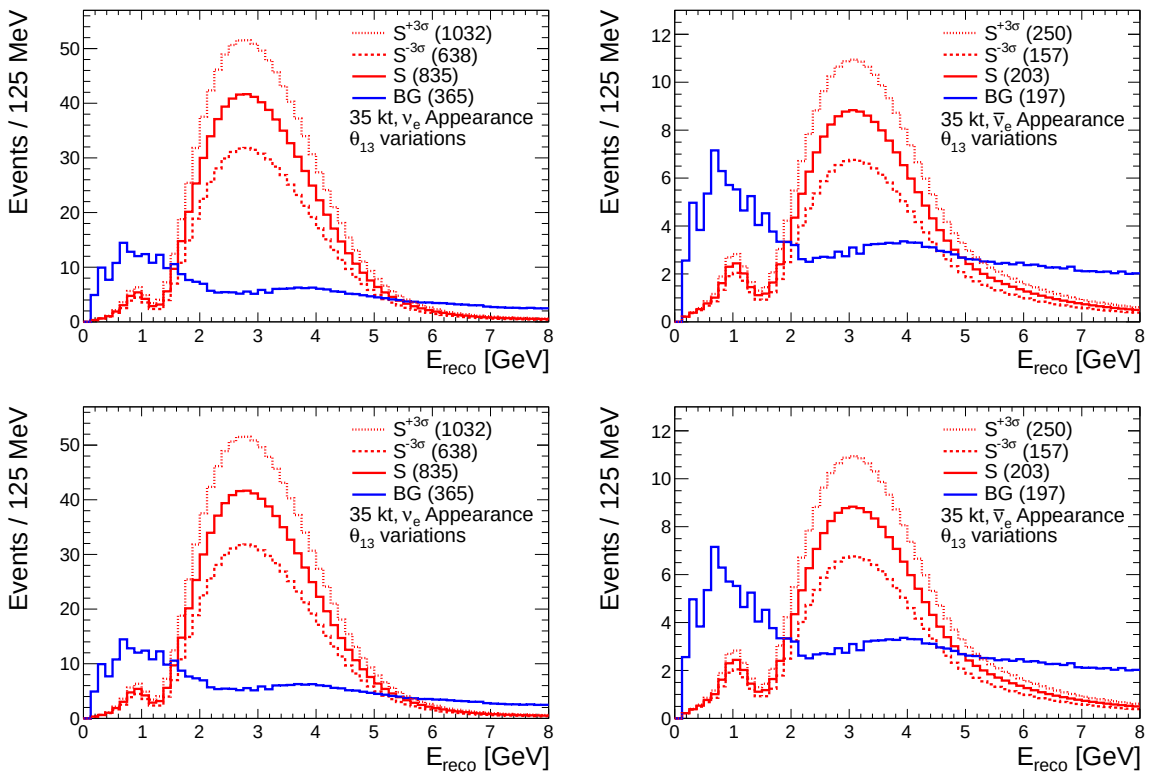


Figure 5: FIXME Real IH plots. Variations in $\theta_{13}$: $\nu_e$ appearance (left) and $\overline{\nu}_e$ appearance (right) spectra produced by GLoBES for a 35-kt LArTPC with 3 years of exposure in an 80-GeV, 1.2-MW beam, for true NH (top) and true IH (bottom). The effect of varying the true value of $\theta_{13}$ within its $3\sigma$ allowed range is shown. The total background, which does not depend on value of $\theta_{13}$ (CHECKME), is overlaid on the signal. The total number of signal and background events are indicated in parenthesis.

## 6 Sensitivity Dependence on $\Delta m^2_{31}$

Figure 10 shows the variation in $\nu_e$ and $\overline{\nu}_e$ appearance signal when the true value of $\Delta m^2_{31}$ is varied within its $3\sigma$ allowed range. Figure 11 shows the variation in MH and CPV sensitivity when $\Delta m^2_{31}$ is varied within its $1\sigma$ and $3\sigma$ allowed range. In each case, the nominal relative constraints on all oscillation parameters, including $\Delta m^2_{31}$, are applied and the normalization constraints are the nominal 1% for signal and 5% for background.

## 7 Sensitivity Dependence on $\delta_{CP}$

The variation in $\nu_\mu$ disappearance, $\overline{\nu}_\mu$ disappearance, $\nu_e$ appearance, and $\overline{\nu}_e$ appearance with variations in the true value of $\delta_{CP}$ is shown in Fig. 3.

## 8 Conclusions

## References

[1] J. Beringer *et al.*, **Particle Data Group** , "Review of Particle Physics (RPP)," *Phys.Rev.* **D86** (2012) 010001.

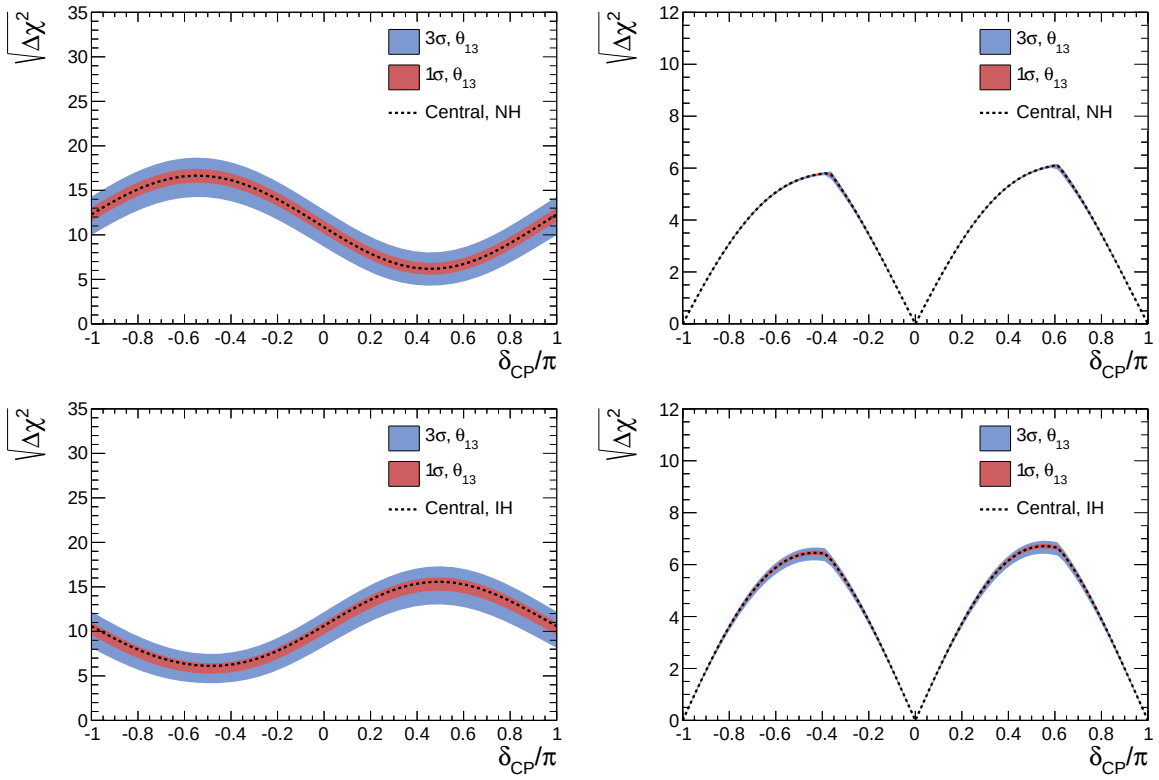


Figure 6: Variations in $\theta_{13}$: MH (left) and CPV (right) sensitivities produced by GLoBES for a 35-kt LArTPC with 3+3 ($\nu + \overline{\nu}$) years of exposure in an 80-GeV, 1.2-MW beam, for true NH (top) and true IH (bottom). The effects of varying the true value of $\theta_{13}$ within its $1\sigma$ (red band) and $3\sigma$ (blue band) allowed ranges are shown.


[2] B. Pontecorvo, "Mesonium and anti-mesonium," *Sov. Phys. JETP* **6** (1957) 429.

[3] B. Pontecorvo, "Neutrino experiments and the problem of conservation of leptonic charge," *Sov. Phys. JETP* **26** (1968) 984.

[4] Z. Maki *et al.*, "Remarks on the unified model of elementary particles," *Prog. Theor. Phys.* **28** (1962) 870.

[5] C. Adams *et al.*, "Scientific opportunities with the long-baseline neutrino experiment.". arXiv:1307.7335.

[6] M. Freund, "Analytic approximations for three neutrino oscillation parameters and probabilities in matter," *Phys.Rev.* **D64** (2001) 053003, `arXiv:hep-ph/0103300 [hep-ph]`.

[7] F. Capozzi, G. Fogli, E. Lisi, A. Marrone, D. Montanino, *et al.*, "Status of three-neutrino oscillation parameters, circa 2013," `arXiv:1312.2878 [hep-ph]`, 2013.

[8] P. Huber, M. Lindner, and W. Winter, "Simulation of long-baseline neutrino oscillation experiments with GLoBES (General Long Baseline Experiment Simulator)," *Comput.Phys.Commun.* **167** (2005) 195, `arXiv:hep-ph/0407333 [hep-ph]`.

[9] P. Huber, J. Kopp, M. Lindner, M. Rolinec, and W. Winter, "New features in the simulation of neutrino oscillation experiments with GLoBES 3.0: General Long Baseline Experiment Simulator," *Comput.Phys.Commun.* **177** (2007) 432–438, `arXiv:hep-ph/0701187 [hep-ph]`.

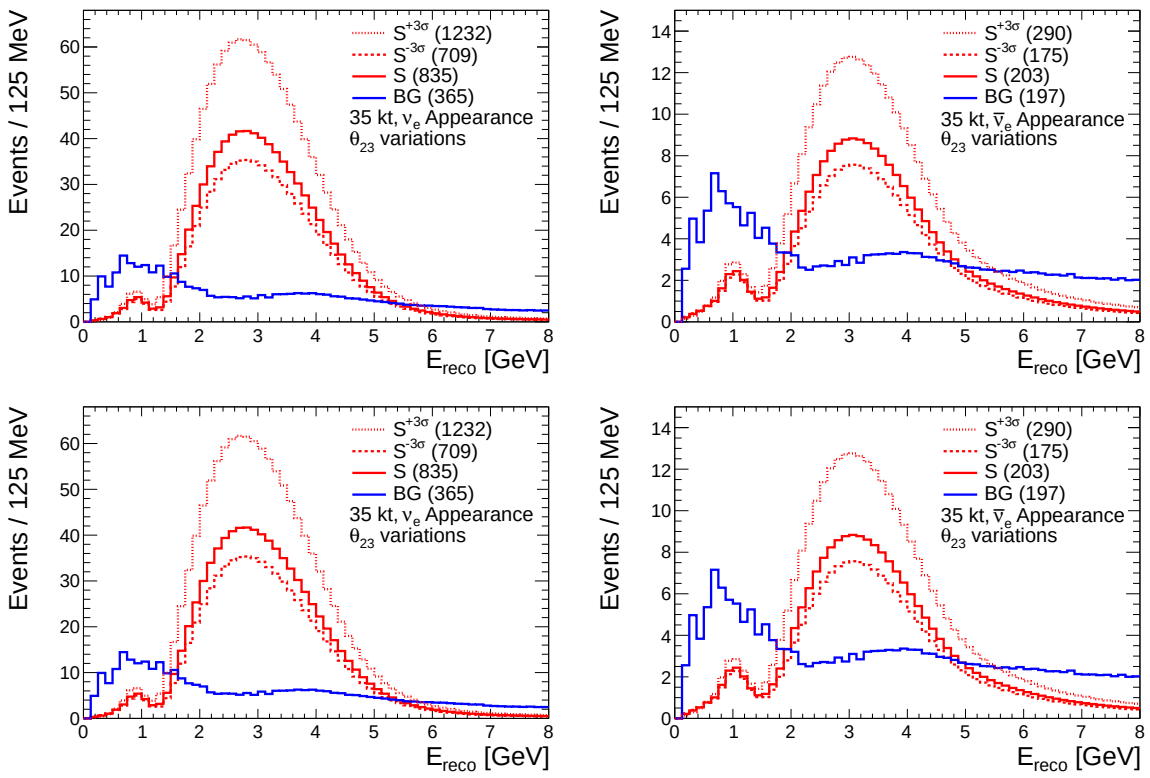


Figure 7: FIXME Real IH plots. Variations in $\theta_{23}$: $\nu_e$ appearance (left) and $\overline{\nu}_e$ appearance (right) spectra produced by GLoBES for a 35-kt LArTPC with 3 years of exposure in an 80-GeV, 1.2-MW beam, for true NH (top) and true IH (bottom). The effect of varying the true value of $\theta_{23}$ within its $3\sigma$ allowed range is shown. The total background, which does not depend on value of $\theta_{23}$ (CHECKME), is overlaid on the signal. The total number of signal and background events are indicated in parenthesis.


[10] C. Andreopoulos, **GENIE Collaboration** , "The GENIE neutrino Monte Carlo generator," *Acta Phys.Polon.* **B40** (2009) 2461–2475.

[11] **ICARUS** . `http://icarus.lngs.infn.it/`.

[12] F. An *et al.*, **Daya Bay Collaboration** , "Spectral measurement of electron antineutrino oscillation amplitude and frequency at Daya Bay," `arXiv:1310.6732 [hep-ex]`, 2013.

[13] G. Fogli, E. Lisi, A. Marrone, D. Montanino, A. Palazzo, *et al.*, "Global analysis of neutrino masses, mixings and phases: entering the era of leptonic CP violation searches," *Phys.Rev.* **D86** (2012) 013012, `arXiv:1205.5254 [hep-ph]`.

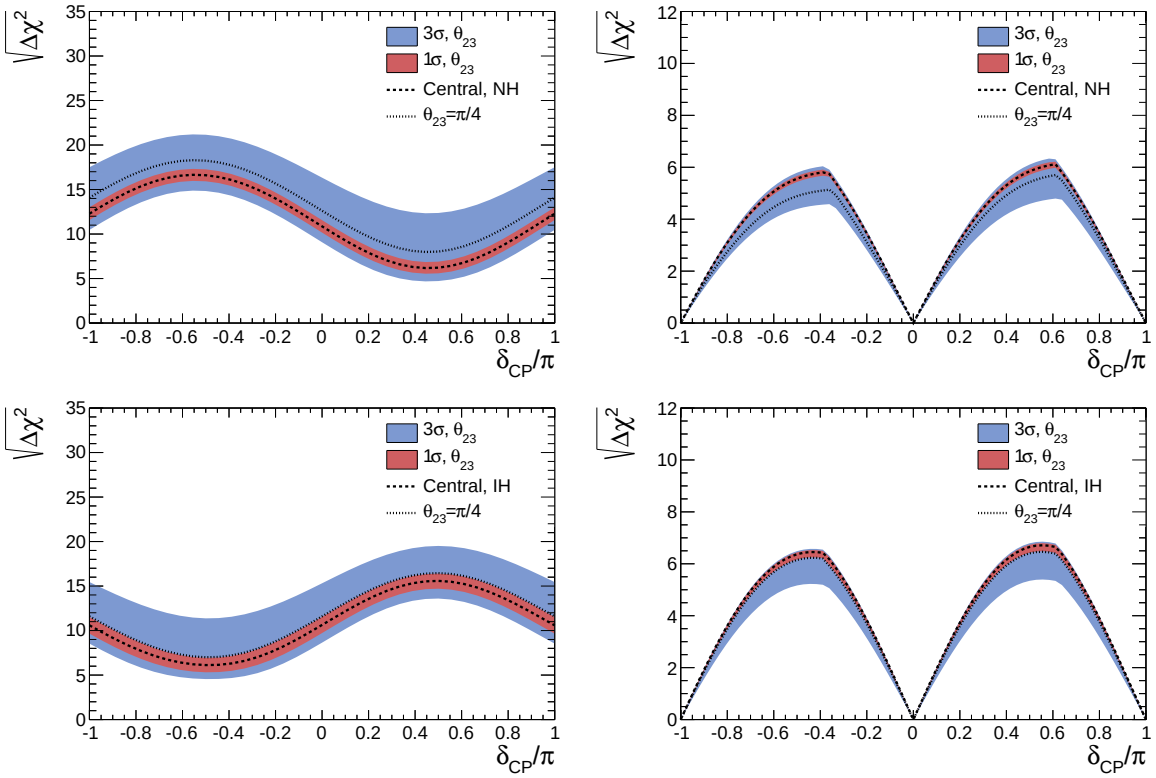


Figure 8: Variations in $\theta_{23}$: MH (left) and CPV (right) sensitivities produced by GLoBES for a 35-kt LArTPC with 3+3 ($\nu + \overline{\nu}$) years of exposure in an 80-GeV, 1.2-MW beam, for true NH (top) and true IH (bottom). The effects of varying the true value of $\theta_{23}$ within its $1\sigma$ (red band) and $3\sigma$ (blue band) allowed ranges are shown. The sensitivities when $\theta_{23} = \pi/4$ (maximal mixing between $\nu_\mu$ and $\nu_\tau$) are also shown.

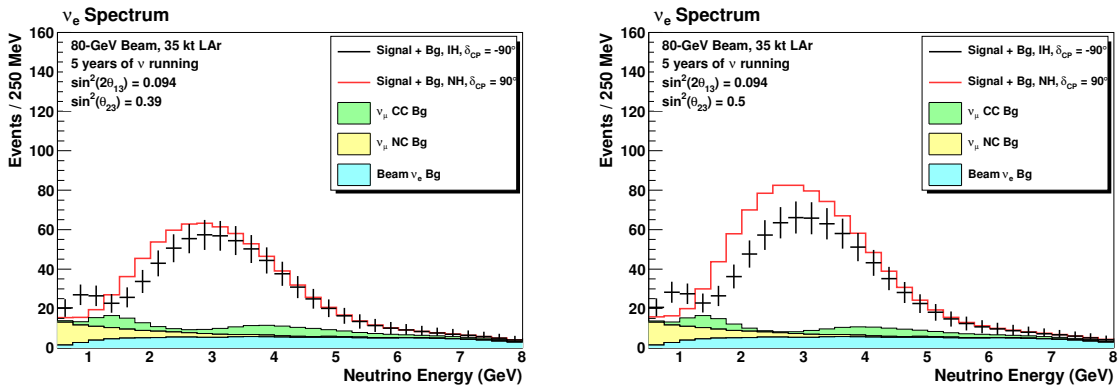


Figure 9: Spectrum for true normal hierarchy and $\delta_{CP} = \pi/2$ (red) compared to the spectrum for true inverted hierarchy and $\delta_{CP} = -\pi/2$ (black), for $\sin^2(\theta_{23}) = 0.39$ (left) and $\sin^2(\theta_{23}) = 0.5$ (right). For the smaller value of $\theta_{23}$ shown on the left, the spectra are quite degenerate. For the larger value of $\theta_{23}$ shown on the right, the degeneracy is broken. Neutrino event spectra are shown for illustration; the degeneracy is also broken in antineutrino spectra.

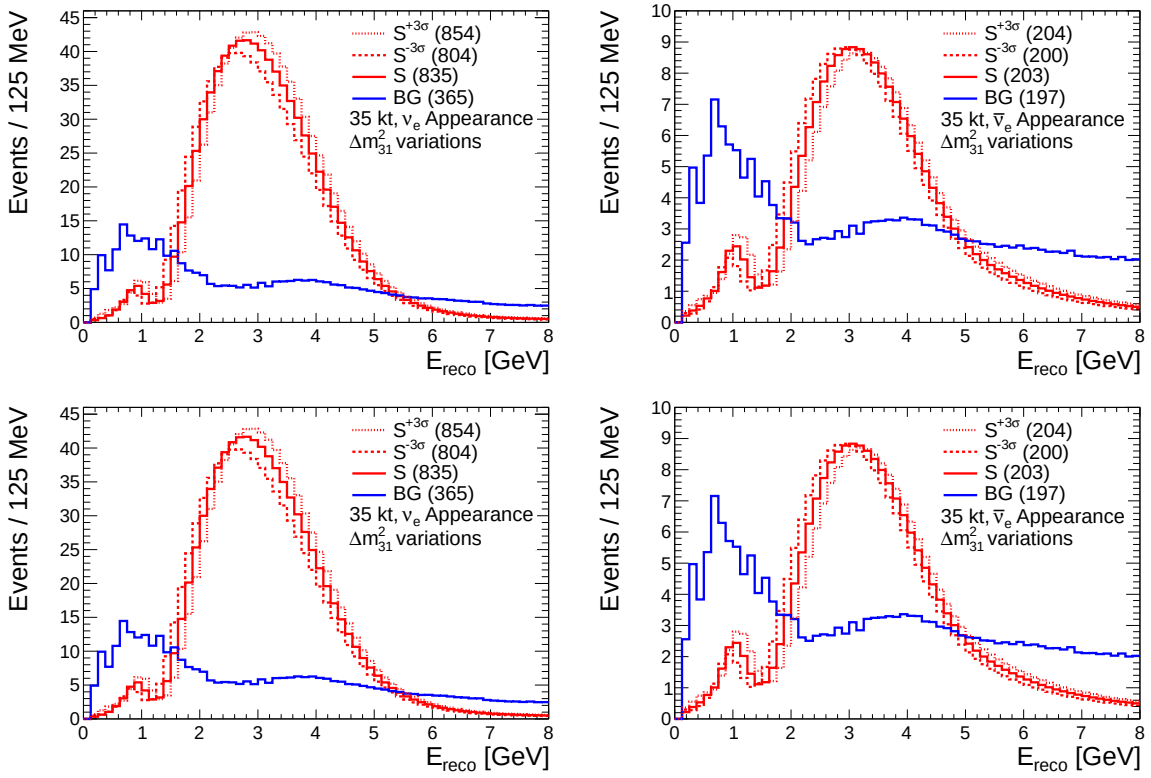


Figure 10: FIXME Real IH plots Variations in $\delta m^2_{31}$: $\nu_e$ appearance (left) and $\overline{\nu}_e$ appearance (right) spectra produced by GLoBES for a 35-kt LArTPC with 3 years of exposure in an 80-GeV, 1.2-MW beam, for true NH (top) and true IH (bottom). The effect of varying the true value of $\Delta,^2_{31}$ within its $3\sigma$ allowed range is shown. The total background, which does not depend on value of $\Delta m^2_{31}$ (CHECKME), is overlaid on the signal. The total number of signal and background events are indicated in parenthesis.

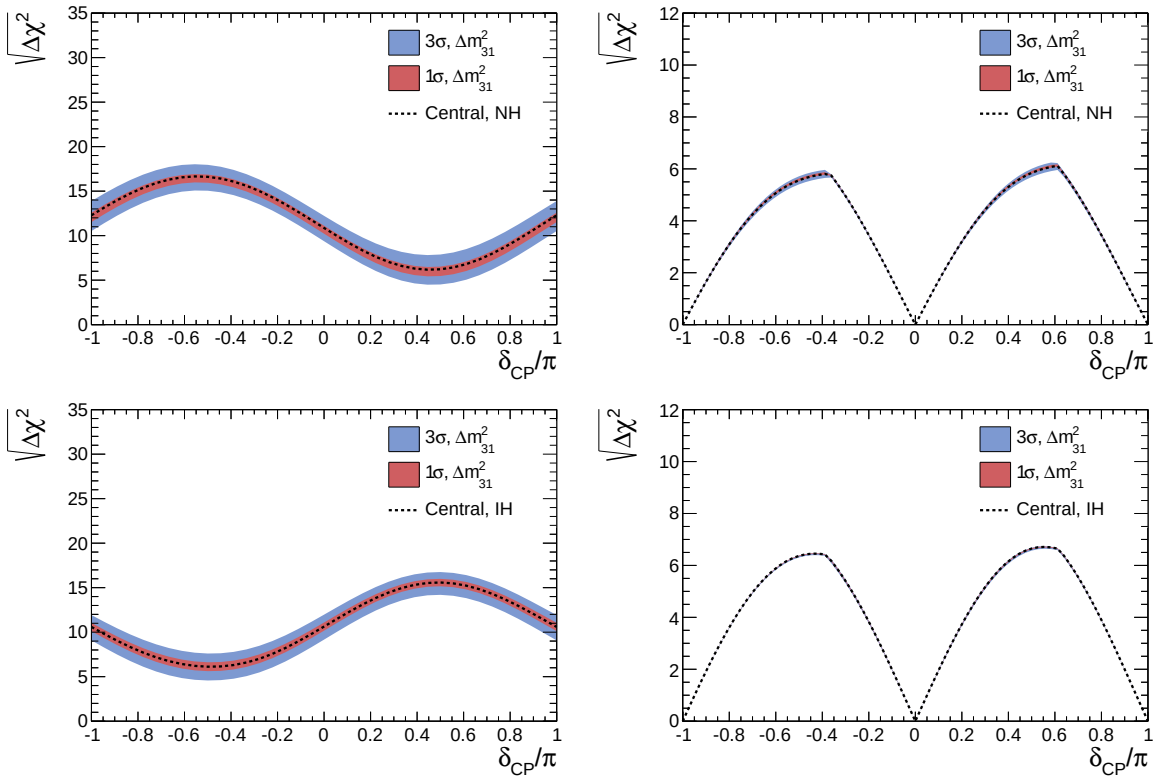


Figure 11: Variations in $\Delta m^2_{31}$: MH (left) and CPV (right) sensitivities produced by GLoBES for a 35-kt LArTPC with 3+3 ($\nu + \overline{\nu}$) years of exposure in an 80-GeV, 1.2-MW beam, for true NH (top) and true IH (bottom). The effects of varying the true value of $\Delta m^2_{31}$ within its $1\sigma$ (red band) and $3\sigma$ (blue band) allowed ranges are shown.

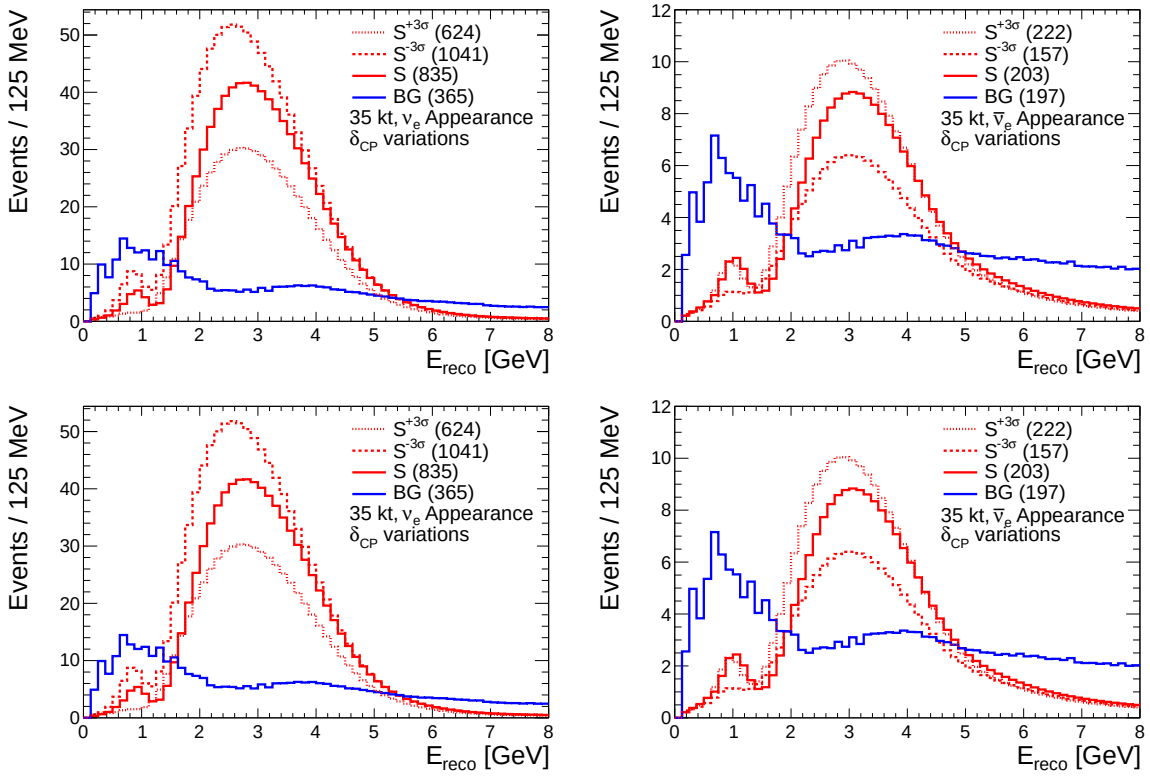


Figure 12: FIXME: Get real IH plots. Variations in $\delta_{CP}$: $\nu_e$ appearance (left) and $\overline{\nu}_e$ appearance (right) spectra produced by GLoBES for a 35-kt LArTPC with 3 years of exposure in an 80-GeV, 1.2-MW beam, for true NH (top) and true IH (bottom). The effect of varying the true value of $\delta_{CP}$ from $-\pi/2$ to zero to $\pi/2$ is shown. The total background, which does not depend on value of $\delta_{CP}$ (CHECKME), is overlaid on the signal. The total number of signal and background events are indicated in parenthesis.